1

Computational Modeling of Abdominal Aortic Aneurysms

Nenad D. Filipovic[1,2]

[1]*Faculty of Engineering, University of Kragujevac, Kragujevac, Serbia*
[2]*Bioengineering Research and Development Center, BioIRC Kragujevac, Serbia*

1.1 Background

Abdominal aortic aneurysm (AAA) is a dilation of the aorta beyond 50% of the normal vessel diameter [1] that is frequently observed in the aging population [2] and it affects 6–9% of the people in the industrialized world. It is a major health problem that typically affects men after the age of 50 [3] and it is the thirteenth leading cause of death in Western societies [4]. AAAs cause about 15 000 deaths per year in the United States only [5], and 1.3% of all deaths among men aged 65–85 years in developed countries [6–8]. In the United States alone, 1.5 million have undiagnosed AAAs [3]. They can remain asymptomatic for most of their development and, if left untreated, they can enlarge and eventually rupture with catastrophic mortality rate of 80% [9] to 90% [2]. On the other hand, the mortality following elective AAA repair has significantly improved to 3–6% [10] which clearly demonstrates the need of diagnosing and monitoring AAAs on time in order to make progress in both medical and economic domain.

A myriad of different factors are established in the literature to account for AAA formation, expansion, and, eventually, rupture. Namely, a substantial amount of research on AAA expansion and rupture focuses on different biological and biomechanical factors and, lately, special attention is put to genes and chemical influences. Among biological factors and risk factors, authors usually discuss the influence of diameter, sex, blood pressure, chronic obstructive pulmonary disease, and smoking [11]. From a biomechanical point of view, major factors contributing to AAA expansion and rupture are the wall stress [12, 13] and strength [14], wall stiffness [15], vessel asymmetry [16–19], intraluminal thrombus (ILT) [20, 21], entire geometry [22, 23], etc. Namely, according to the biomechanical perspective,

Computational Modeling and Simulation Examples in Bioengineering, First Edition. Edited by Nenad D. Filipovic.
Published 2022 by John Wiley & Sons, Inc.

AAA rupture is usually defined as a material failure of the degenerated AAA wall to withstand the stress exerted on it [24]. However, the relationship between rupture and biomechanics of aorta proved to be more complex [10] and the evaluation based only on one of these parameters is not sufficient.

For many years, diameter was taken to be the primary parameter associated with rupture risk estimation. Namely, the threshold of $\geq 5.5\,cm^3$ was applied as indicative for AAA repair [10]. However, continuous studies in the past showed that while 10–24% of small aneurysms (<5.5 cm) may rupture [1], aneurisms which diameter exceeds the threshold remain stable. These findings cast doubt over the suitability of surgical repair based solely on the maximum diameter criterion [16–18]. In order to refute "diameter criterion" rule, many other criteria and parameters ensued. In contrast, the survey conducted in 2006 [25] confirmed that 92% of surgeons still use maximum diameter criterion and growth rate in making decisions about the surgical intervention while 19% of them stated that they were not even aware that biomechanics may influence the rupture risk. The results of the survey suggest that cooperation of surgeons and engineers is necessary in order not just to make technical advances but to implement them in practice.

Mutual collaboration of clinicians and engineers resulted in different efforts and methodologies proposed in the last few decades, all striving to make progress in the domain of AAA expansion and rupture prediction. This paper reviews some of the most significant studies in the area of AAA modeling in the past decades which further understanding of utmost importance for making additional progress toward validation and application in the clinical setting. We firstly described computational methods applied for AAA in chronological order. Then, different experimental testing as well as our own testing is described in order to determine the mechanical properties of AAA. Mechanical–chemical including ILT modeling is separately analyzed. Finite element procedure including fluid–structure interaction (FSI) from our group is described. In the end, some of data mining (DM) approach and vision for future clinical decision support system (DSS) is given.

1.2 Clinical Trials for AAA

The known risk factors for AAA include male sex, smoking, hypertension, and a family history of AAA in a first-degree relative [26]. Many clinical studies confirmed that smoking is the most important modifiable risk factor for AAA [27–33]. Some authors discovered that the duration of smoking and daily cigarette number are also associated with a higher risk of AAA [28, 34]. One large systematic review of studies evaluating smoking and aortic aneurysm placed the relative risk of aortic aneurysm-related events in current smokers between 3 and 6 [34].

Smoking contributes significantly to the prevalence of AAA and may account for 75% of all AAA, 4 cm in diameter or larger [33].

A history of hypertension and myocardial infarction or coronary artery bypass surgery was negatively associated, whereas a body mass index $\geq$25 kg/m^2 was protective [35].

1.3 Computational Methods Applied for AAA

The study of Darling et al. [36] was one of the first studies to conclude that AAA rupture predominately occurs on posterior walls. Namely, in the autopsy study conducted almost 40 years ago on AAA patients, among whom 473 died with surgically intact arteriosclerotic AAAs, it was reported that 82% of ruptures occurred along the posterior and posteriolateral wall of AAA. Consequently, it was important to examine the wall stress acting on these regions in AAA, so that many studies were influenced to direct their research toward examining posterior wall stress for clinical relevance. One of the first studies to apply the finite element analysis (FEA) to determine the AAA wall stress was the study of [37] who concluded that FEA has a potential of becoming a crucial tool in the study of vascular mechanics. Their study was followed by extensive research in the area of numerically predicted AAA wall stress that continues even at present. However, limitations of this study include the use of idealized models with regular structures and evenly distributed wall stress.

In 1998, Vorp et al. [38] published a study on the influence of maximum diameter and aortic aneurysm asymmetry on mechanical wall stress. They investigated the effects of asymmetry on 3D stress distribution in the wall of AAA and refuted the critical diameter criterion suggesting that all AAAs with the same diameter have the same risk of rupture. They generated 10 virtual computer models with commercial software (Pro-Engineer v. 16.0; Parametric Technology Waltham, Mass) according to two protocols. In the first protocol, five models were generated with constant maximum diameter parameter (6 cm) while asymmetry β varied from 0.3 to 1.0. In the second protocol, asymmetry was kept constant $\beta = 0.4$ while maximum diameter parameter varied from 4 to 8 cm. The results confirmed that both parameters had the influence on the increase and decrease in the wall stress in the different sections of the aneurisms and that aneurysm rupture was caused by a gross mechanical failure of the aortic wall which occurs when wall stress exceeds the strength of the tissue. It was also concluded that maximum stress occurs on the posterior wall for small AAAs ($\leq$5), while for larger AAAs peak stress is on the anterior surface. Although it pioneered in proving the effects of asymmetry, the study was performed on virtual models, so potential limitations assuming that

AAA wall is homogenous, isotropic, and linearly elastic with small strains and uniform thickness have to be taken into account when analyzing real AAA models.

Venkatasubramaniam et al. [10] refuted traditional views that relate aneurysm size to the risk of rupture. They conducted a comparative study of aortic wall stress in ruptured and non-ruptured aneurysms with an aim to prove the importance of wall stress when predicting the risk of rupture in individual patients. Namely, the study included computed tomography (CT) scans of 27 patients (12 ruptured and 15 non-ruptured AAA), predominantly males. Using the finite element method, they calculated wall stress using the geometry of AAA, the material properties of the aortic wall, and the forces and constraints acting on the wall. The material properties were used from a previously validated mathematical model by [39–41]. ANSYS 6.1 program (ASN Systems Ltd, Cannonsburg, USA) was utilized for the analysis and post-processing while the von Mises stress was used to evaluate the state of the aneurysms. There were no important differences in the mean diameter between two groups (6.8 cm for non-ruptured and 7.6 cm for ruptured, $P > 0.1$) and there were two aneurysms that ruptured at small diameters of 5.0 and 5.7 cm. The authors concluded that AAA that ruptured or went on to rupture had significantly higher peak stress (mean 1.02 MPa) compared with non-ruptured (mean 0.62 MPa). Moreover, systolic blood pressure was also significantly higher in ruptured AAA. Noting that 45 and 65 mm diameter AAAs can have the same stress, they emphasized the role of the shape and asymmetry of the aneurism including the anterior and superior limits. They also demonstrated that wall stress can be calculated from a routine CT scan and that it may be a better predicator of AAA risk of rupture than diameter alone on the individual basis. On the other hand, the study assumed a uniform AAA wall thickness of 2 mm and did not take into account the effect of thrombus on wall stress.

In 2006, Vande Geest et al. [42] developed a biomechanics-based rupture potential index (RPI) that became a useful rupture prediction tool. Namely, the RPI predetermined the wall strength on a patient-specific basis by utilizing experimental tensile testing and statistical modeling. The tissue strength was calculated by taking parameters such as age, sex, smoking status, family history of AAA, normalized diameter, and the maximum thickness of the ILT into account. Then, the wall stress was predicted with FEA. Although the authors reported that the RPI has a potential to identify high rupture risk of AAA better than diameter or peak wall stress (PWS) alone, their approach still requires validation before it can be introduced into clinical setting.

In the study conducted by Scotti et al. [43], 10 idealized models of AAA were used, generated with the CAD software ProEngineer Wildfire (Parametric Technology Corporation, Needham, MA) [44] together with an additional nonaneurismal model as control in order to assess the significance of an arbitrary estimated peak fluid pressure (117 mmHg) compared with nonuniform pressure

resulting from a coupled FSI. The models differed in the degree of asymmetry and wall heterogeneity and the FEA was used to estimate the effects of asymmetry and wall thickness on the wall stress and fluid dynamics. Each model contained fluid and solid domain and was analyzed with static pressure-deformation analysis together with FSI. The Navier–Stokes equations were used as governing equations for homogeneous blood flow, while for computational solid stress (CSS) analysis, only the solid domain was considered. The results exhibited that a realistic fluid pressure distribution to the inner AAA wall (instead of an arbitrary peak systolic pressure) resulted in at least 20% higher wall stress, despite wall thickness heterogeneity. Additionally, maximum AAA wall stress increased with asymmetry although the computational model included blood flow.

Finol and Ender [45, 46] used a Spectral Element Method with three-step time splitting scheme for the semidiscrete formulation of the time-dependent terms in the momentum equations for axisymmetric two-aneurysm abdominal model. This methodology has been widely used for the Direct Numerical Simulation of transitional flows with fast-evolving temporal phenomenon and complex geometries.

Multi-scale models for AAA are considered constitutive models for vascular tissue, where collagen fibers are assembled by proteoglycan cross-linked collagen fibrils (CFPG-complex) and reinforce an otherwise isotropic matrix (elastin). There is multiplicative kinematics for the straightening and stretching of collagen fibrils. Mechanical and structural assumptions at the collagen fibril level define a piece-wise analytical stress–stretch response of collagen fibers.

The concept of multi-scale constitutive model performs integration at the material point for macroscopic stress which takes into account micro plane concept incorporated in the finite element modeling (FEM) [47, 48].

Zhang et al. [49] used multi-scale and multi-physical models for understanding disease development and progression, and for designing clinical interventions. They investigated multi-scale models of cardiac electrophysiology and mechanics for diagnosis, clinical decision support, and personalized and precision medicine in cardiology with examples in arrhythmia and heart failure.

FSI describes the wave propagation in arteries driven by the pulsatile blood flow. These problems are complex and challenging due to the high nonlinearity of the problem. The nonlinearity exists in the fluid equation but also in the structure displacement which modifies the fluid domain and generates geometrical nonlinearities as well [50].

Some authors used the generalized string model as the structure of blood flow in compliant vessels and arteries [50–56]. Causin et al. [57] described this string model as a structural model derived from the theory of linear elasticity for a cylindrical tube with small thickness. Nobile and Vergara [56] emphasized that the generalized string model neglects bending as well. Čanić et al. [58–61] claimed that there are no analytical results which are able to prove the well posedness of FSI

problems without assuming the structure model that includes the higher-order derivative terms, capturing the viscoelastic behavior. For blood flow, there is a strong added mass effect issue in which the fluid and structure have comparable densities.

All the above studies demonstrate the importance of biomechanical modeling of AAA by using FEM approach with and without FSI and nonlinear wall deformation. This mechanical approach provides an additional understanding of potential indicators of rupture risk.

1.4 Experimental Testing to Determine Material Properties

Experimental tests are used to determine the mechanical properties of AAA. In-vivo measurements are based on the imaging modality. For in-vivo measurements, the main difficulty is to accurately determine the true force and the displacement distribution for the aorta wall. For isolating samples often unknown changes of their behavior affecting the results of such tests. MacSweeney et al. [62] found that elastic modulus was higher in aneurysmal abdominal aorta compared with controls. More recently, van't Veer et al. [63] estimated the compliance and distensibility of AAA by means of simultaneous instantaneous pressure and volume measurements obtained with the magnetic resonance imaging (MRI). Ganten et al. [64] by using time resolved electrocardiography (ECG)-gated CT imaging data from 67 patients, found that the compliance of AAA did not differ between small and large lesions. Molacek et al. [65] did not find any correlation between aneurysm diameter and distensibility of AAA wall and of normal aorta. Uniaxial extension testing is the simplest and most common of *ex-vivo* testing methods. The recorded force-extension data are converted to stress/strain. Di Puccio et al. [66] provided a recent review of the incompressibility assumption on soft biological tissue. Biaxial test was used as an initial square thin sheet of material which is stress normally to both edges. Even this test is not sufficient to fully characterize anisotropic materials [67, 68], although it can capture additional information regarding the mechanical behavior of the specimens with respect to uniaxial one.

One of the most complete data for biaxial mechanical behavior of aorta and AAAs is described in Vande Geest et al. [69, 70]. They reported on biaxial mechanical data for AAA (26 samples) and normal human AA as a function of age: less than 30, between 30 and 60, and over 60 years of age. They found that the aortic tissue becomes less compliant with age and that AAA tissue is significantly stiffer than normal abdominal aortic tissue.

At Clinical Center in Belgrade, Serbia, we developed an experimental procedure for bubble inflation test. Intraoperatively, specimens of anterior wall of AAA are harvested, stored in saline at 4° C immediately, and placed in the laboratory setup that simulates natural forces by exposing aortic tissue specimen to inflation with pressurized solution [71] (Figure 1.1). The model consists of the mechanical pump with Crebs–Ringer solution, heater and heat exchanger, tissue container, pressure sensor, and transducer with camera. Camera and pressure transducer system were connected by USB connection with the laptop serving as a control unit and data collector. After heating the Crebs–Ringer solution in the system to 37 °C, the pump was turned on and the pressure was gradually increased exposing aortic tissue to the maximum pressure until the moment of tissue rupture that was recorded by a webcam placed above the tissue. Pressure value in the moment of rupture was known due to the dedicated software defining tissue (failure) strength.

Ex-vivo testing is mostly based on uniaxial or biaxial stretching of the intraoperatively harvested tissue specimens. These tests have the ability to characterize intrinsic properties of the tissue itself with independent physical meanings, stiffness, failure stress, and strain. Tissue sample is exposed to extension along its length at a constant displacement rate, while the force is recorded during extension and until failure of the tissue. Uniaxial extension testing is the simplest and most common. Van de Geest et al. [72] reported uniaxial extension testing of 69 AAA specimens, from 21 patients. A novel mathematical model to estimate physically meaningful measures such as stiffness varied from 21.2 to 19.3 N/cm^2, mean 80.5 N/cm^2.

Improvement of uniaxial testing was achieved by performing biaxial testing, when specimen is exposed to determined forces between the two orthogonal directions. Using biaxial testing, the same authors compared the tissue of AAA and normal aorta and compared their behavior in longitudinal and circumferential direction. They found that aneurysmal degeneration of the abdominal aorta is associated with an increase in mechanical anisotropy, with preferential stiffening in the circumferential direction. Information related to stiffness and strain of aortic tissue was gained. Thubrikar et al. [73] were testing different regions of aneurysm in terms of yield stress, yield strains, and other mechanical properties, and found that the anterior wall of AAA is the weakest. In the circumferential direction, the yield stress of the lateral region was greater than that of the anterior or posterior region ($73 + 22$ N/cm^2 versus $52 + 20$ N/cm^2 or $45 + 14$ N/cm^2, respectively).

Our results showed rupture of the tissue at the inflation pressure of 9.8 N/cm^2. The analytical calculated wall strength for wall thickness 0.2 cm and aorta radius 1 cm was 24.5 N/cm^2. FEA showed PWS of 57 N/cm^2 and wall stress of 21.2 N/cm^2 at the anterolateral wall of AAA in the area of harvested tissue [71].

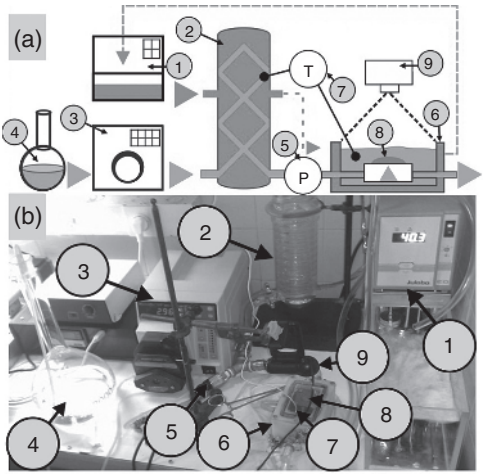

Figure 1.1 (a) Cartoon schema. (b) Real laboratory model. Laboratory model consists of the mechanical pump (3) with Crebs–Ringer solution (4), heater (1) and heat exchanger (2), tissue container (6), pressure sensor (5), and transducer with camera (9). Camera and pressure transducer system were connected by USB connection with the laptop serving as a control unit and data collector. After heating the Crebs–Ringer solution in the system to 37 °C (7 – temperature sensor), the pump was turned on and the pressure was gradually increased exposing aortic tissue (6) to the maximum pressure until the moment of tissue rupture that was recorded by a webcam placed above the tissue. Pressure value in the moment of rupture was known due to the dedicated software defining tissue (failure) strength.

1.5 Material Properties of the Aorta Wall

It is very important to use arterial wall with proper material model because the wall stiffness increases when lumen diameter increases and calcification and medial sclerosis occur with aging and disease. The aneurysmal wall has been found to be mechanically anisotropic [74]. Isotropic properties assumption is a reasonable assumption in most cases. A more accurate constitutive model is needed to describe the properties of the wall.

The flat arterial tissue layer is assumed to be a fiber-reinforced material with relatively stiff collagenous fibers embedded in a homogeneous isotropic (soft) ground matrix [75]. The assumption of strain energy functions holds good only for single continuous medium tissues which is not the case with arterial tissue [76]. The mechanical properties of soft biological tissues depend greatly on their microstructure integration attained in the constitutive model [49]. Taghizadeh et al. [77] proposed a new biaxial constitutive model based on microstructural properties as opposed to the simple uniaxial tests carried out by Sokolis et al. [78] and Karimi

et al. [79]. Wall thickness is also very important. Since aneurysmal rupture occurs at a specific site of the aortic lumen, the properties of the wall affect the computed solution. The aortic wall thickness in computational methods is assumed to be in the range of 1.5–2 mm. While this may be largely accurate for most simulations, it has been acknowledged as a major limitation in the completeness of the prediction solution [80]. Raut et al. [81] suggested that the wall thickness as a constant value is not accurate and described a novel method that incorporated the regionally varying wall thickness, especially in the area of rupture.

1.6 ILT Modeling

Most aneurysms have ILT within their lumen. Stenbaek et al. [82] described that the development of ILT may be a better predictor than the maximum diameter of the AAA as a rupture risk parameter. Li et al. [83] calculated that the non-ILT models had higher stress development than the ILT models. Di Martino and Vorp [84] found that ILT might protect the AAA wall from the pressure applied by blood flow. O'Leary et al. [85] performed mechanical tests on 356 samples and classified them into 3 morphologies, type 1 which was a multilayered ILT which strength and stiffness decreased gradually, type 2 which strength decreased abruptly, and a single-layered ILT with lower strength and stiffness compared with the other two types. Tong et al. [86] carried out biomechanical behavioral studies on 90 AAA samples (78 men and 12 women). They found that the female ILT luminal layer showed a lower stiffness in the longitudinal direction than male and, consequently, the thrombi may have different wall weakening effects in males and females. Speelman et al. [87–89] also showed that AAA wall stress is closely related to the AAA diameter. Namely, they investigated whether wall stress can be used to predict stable and progressive AAAs as well as the effect of ILT on wall stress. The study was conducted on the finite element models of 30 patients with wall stresses computed with and without ILT for stable and progressive AAAs. The results showed that ILT reduced AAA wall stress, progressive AAA growth was not related to the diameter but AAA volume and relative ILT volume, and that higher wall stress was related to AAA growth only when ILT was not included in the simulations.

Kontopodis et al. [90] analyzed a single uncommon case of a 75-year-old Caucasian male diagnosed with fast-growing AAA without family history but with other medical conditions such as smoking, hypertension, diabetes, and COPD. The aneurism which was initially small (45 mm in diameter) presented a growth of 1 cm in only six months. The focus of research was on thrombus and lumen volumes, thrombus maximum thickness, maximum centerline curvature together

with biomechanical aspects such as PWS and areas with high stress and stress redistribution. Two 3D AAA models (initial and follow up) were reconstructed from 2D CT angiography images with manual and automatic segmentation process performed with open source software ITK-SNAP [91]. The results indicated that the total volume increased from 85 to 120 ml for six months while lumen volume remained constant (72 ml for initial and 71 for follow up examination). Moreover, ILT increased from 14 to 50 ml and maximum thickness increased from 0.3 to 1.6 cm in the anterior part with maximum curvature of the centerline increased from 0.4 to 0.5 cm^{-1} suggesting an anterior bulging. Additionally, area under high wall stress remained almost constant while there was a marked redistribution of wall stress from anterior site and AAA neck to posterior wall. Total posterior wall area exposed to stress was 0 cm^2 at the initial stage and 9.7 cm^2 at the follow up. It was interesting to note that PWS did not increase as was the case with previous studies (e.g. [89]). Authors suggested that although large-scale studies are needed, information gathered by the analysis could be of use in determining AAA natural history and patient-specific rupture risk estimation. Anton et al. [92] provided an insight into a comparative study, numerical and experimental, to analyze the pressure field in AAA models and validate numerical model's ability to predict experimental pressure field. They used patient-specific AAA geometry with and without ILT with iliac arteries included. Iliac arteries were taken into account because numerical observations suggest that their inclusion is critical for accurate prediction of pressure, flow pattern, and wall stress [93]. Four CFD mathematical models were employed for ILT models and three CFD models were used for model without ILT because Reynolds Stress Model did not converge satisfactorily. CFD models predicted pressure fields substantially well with average difference of 1.1% for the model without ILT and 15.4% for ILT model. Moreover, they aimed to compare the spatial pressure drop before and after the formation of ILT although only few studies before performed spatial pressure drop measurements in AAA (e.g. [94, 95]). The special pressure drop in the ILT model was 5000 Pa while in the model without ILT, it was around 1500 Pa which is explained by the fact that with smaller lumen, flow velocities are higher. The study of Polzer et al. [96] broadened finite element single-phase AAA models (e.g. [69, 97–100]) with poroelastic description of ILT. The model was loaded by a pressure step and a cyclic pressure wave. The numerical results of the studied idealized axisymmetric two-phase AAA models proved that the entire blood pressure was transmitted to the AAA wall in spite of the existence of the ILT, which was also previously confirmed by [101]. The study found that the stress in the AAA wall, at steady state, did not depend on the permeability of ILT and did not differ from single-phase conventional models. Consequently, the results of the study suggested that single-phase description could be used reliably to predict the stress in AAA wall instead of biphasic one which is less computationally efficient. The study also showed that ILT reduced wall tensile stress by a value between 46 and 62%. Additionally, the analysis helped

the explanation of differences between in-vivo and in-vitro measurements by demonstrating that pressure under ILT depends on the local geometry of the AAA. On the other hand, poroelastic description cannot be replaced when investigating transport phenomena through AAA tissue. Baek et al. [102] used a set of 39 patients' CT images data from 9 different patients. The images were divided into two groups – low and high ILT group, so that the effect of ILT on the AAA expansion could be established. The results indicate that the relationship between AAA expansion rate and maximum diameter can be changed by inhomogeneous distribution of ILT thickness. Although generally ILT presence is associated with aneurysm expansion rate, a slowdown of expansion was established in areas of thick ILT.

By using an inverse optimization method, Zeinali and Baek [103] created a computational framework toward patient-specific AAA modeling. Namely, using a 3D geometry from medical images, they identified initial material parameters for healthy aorta to satisfy homeostatic condition and then created different computational shapes and considered multiple spatiotemporal forms of elastin degradation and stress-mediated collagen turnover. The results exhibited the importance of the role of elastin damage extent, geometric complexity of an enlarged AAA, and sensitivity of stress-mediated collagen turnover on the wall stress distribution and the rate of expansion. Also, the study showed that the distributions of stress and local expansion initially correspond to the extent of elastin damage, but change because of stress-mediated tissue growth and remodeling dependent on the aneurysm shape. The specificity of their study lies in the fact that the authors did not use AAA patient-specific model, but medical images of a healthy subject. On the other hand, they suggest that in spite of the model used for the present study, their computational framework could be used in a patient-specific modeling to predict AAA shape and mechanical properties if improved in the domain of boundary conditions, description of aortic tissue, growth and remodeling, and the development of inverse scheme using AAA patients' longitudinal images.

The studies continuously prove that ILT has the potential to influence AAA both biochemically and biomechanically. Namely, ILT induces localized hypoxia, possibly leading to increased neovascularization, inflammation, and local wall weakening [104]. On the other hand, ILT development is strongly influenced by agonists and antagonists of platelets activation, aggregation, adhesion, and the proteins involved in the coagulation cascade which are not thoroughly discussed in the present literature. The study of Biasetti et al. [105] analyzed the evolution of chemical species involved in the coagulation cascade, their relation to coherent vertical structures, and the possible effect on ILT development. The authors developed a fluid–chemical model that simulates the coagulation cascade through a series of convection–diffusion–reaction equations. They followed the coagulation cascade model ([106]) which consisted of 18 species and involved plasma-phase and surface-bound enzymes and zymogens, with both plasma-phase and membrane-phase reactions. Blood was modeled as a non-Newtonian incompressible

fluid. The coupling was achieved by a set of convection–diffusion–reaction equations that were added to the computed blood flow field in order to predict the distribution of chemicals. Since the model was able to couple the fluid and chemical domains, it represents an integrated mechanochemical potential for further understanding of ILT formation and development mechanisms.

Meaningful limitation of the study is mirrored in the fact that authors assumed a rigid wall which may alter the results since ILT tissue can deform during a cardiac cycle and consequently influence the fluid dynamics and the distribution of chemicals.

1.7 Finite Element Procedure and Fluid–Structure Interaction

Blood flow in aorta has a time-dependent 3D flow, so the time-dependent and full three-dimensional Navier–Stokes equations were solved. The laminar flow condition appropriate for this type of analysis [107] was used. The finite element code was validated using the analytical solution for shear stress and velocities through the curved tube [108]. A penalty formulation will be used [109]. The incremental–iterative form of the equations for time step and equilibrium iteration "i" is:

$$\begin{bmatrix} \frac{1}{\Delta t}\mathbf{M_v} + {}^{t+\Delta t}\mathbf{K}_{\mathbf{vv}}^{(i-1)} + {}^{t+\Delta t}\mathbf{K}_{\mu\mathbf{v}}^{(i-1)} + {}^{t+\Delta t}\mathbf{J}_{\mathbf{vv}}^{(i-1)} & \mathbf{K_{vp}} \\ \mathbf{K}_{\mathbf{vp}}^{\mathbf{T}} & \mathbf{0} \end{bmatrix} \begin{Bmatrix} \Delta\mathbf{v}^{(i)} \\ \Delta\mathbf{p}^{(i)} \end{Bmatrix} = \begin{Bmatrix} {}^{t+\Delta t}\mathbf{F}_{\mathbf{v}}^{(i-1)} \\ {}^{t+\Delta t}\mathbf{F}_{\mathbf{p}}^{(i-1)} \end{Bmatrix} \tag{1.1}$$

The left upper index "$t + \Delta t$" denotes that the quantities are evaluated at the end of time step. The matrix $\mathbf{M_v}$ is mass matrix, $\mathbf{K_{vv}}$ and $\mathbf{J_{vv}}$ are convective matrices, $\mathbf{K_{\mu v}}$ is the viscous matrix, $\mathbf{K_{vp}}$ is the pressure matrix, and $\mathbf{F_v}$ and $\mathbf{F_p}$ are forcing vectors. The pressure is eliminated at the element level through the static condensation. For the penalty formulation, the incompressibility constraint is defined in the following manner:

$$\mathrm{div}\mathbf{v} + \frac{p}{\lambda} = 0 \tag{1.2}$$

where λ is a relatively large positive scalar so that p/λ is a small number (practically zero).

1.7.1 Displacement Force Calculations

Displacement force was calculated from direct integration of the pressure and wall shear stress distributions on the surfaces of the aortic wall:

$$\sum F = \int p\mathrm{d}A + \int \tau \mathrm{d}A + F_{\mathrm{g}} \tag{1.3}$$

where the integrals are surface finite elements along the surface of the aortic wall. Weight of blood in standing or supine position was also considered. It was assumed that all of the weight of the blood is supported by the endograft.

1.7.2 Shear Stress Calculation

At the regions of stasis and flow reversals, there is an important role of motion and deformation in the shear stress calculation [110, 111], concept of the rigid wall condition was assumed due to the negligible effect of shear stress on total DF [112]. The distribution of stresses within the blood was estimated. The stresses ${}^{t}\sigma_{ij}$ at time "t" is equal

$${}^{t}\sigma_{ij} = -{}^{t}p\delta_{ij} + {}^{t}\sigma_{ij}^{\mu} \tag{1.4}$$

where

$${}^{t}\sigma_{ij}^{\mu} = {}^{t}\mu^{t}\left(v_{i,j} + v_{j,i}\right) \tag{1.5}$$

is the viscous stress, ${}^{t}\mu$ is viscosity corresponding to the velocity vector ${}^{t}\mathbf{v}$ at a spatial point within the blood domain. The viscous stresses are represented by (1.5).

The wall shear stress is calculated as:

$${}^{t}\tau = {}^{t}\mu\frac{\partial^{t}v_{t}}{\partial n} \tag{1.6}$$

where ${}^{t}v_{t}$ denotes the tangential velocity, and n is the normal direction at the vessel wall. At the integration points near the wall surface, the tangential velocity was estimated first, and then the velocity gradient $\partial^{t}v_{t}/\partial n$ was calculated. Finally, the viscosity coefficient ${}^{t}\mu$ using the average velocity was evaluated. Blood was taken as an incompressible Newtonian fluid, appropriate for larger arteries [110]. The kinematic viscosity was $\nu = 3.5\mathrm{e}{-6}\,\mathrm{m}^2/\mathrm{s}$ and the blood density was $\rho = 1050\,\mathrm{kg/m}^3$.

1.7.3 Modeling the Deformation of Blood Vessels

In modeling blood flow in large blood vessels, we have recognized two distinct cases: (i) rigid walls and (ii) deformable walls. The assumption (i) is mostly adopted in practical applications. It is very important to determine the stress–strain state in tissue, when blood and blood vessel system is analyzed, as well as the effects of the wall deformation on the blood flow characteristics.

There are complex mechanical characteristics of blood vessel tissue. The tissue can be modeled from linear elastic to nonlinear viscoelastic model. The governing

finite element equations used in modeling wall tissue deformation with emphasis on implementation of nonlinear constitutive models are summarized.

If the principle of virtual work is applied, the differential equations of motion of a finite element are

$$\mathbf{M}\ddot{\mathbf{U}} + \mathbf{B}^{w}\dot{\mathbf{U}} + \mathbf{K}\mathbf{U} = \mathbf{F}^{\text{ext}} \tag{1.7}$$

where the element matrices are: $\mathbf{M}$ is mass matrix; $\mathbf{B}^{w}$ is the damping matrix, in case when the material has a viscous resistance; $\mathbf{K}$ is the stiffness matrix; and $\mathbf{F}^{\text{ext}}$ is the external nodal force vector which includes body and surface forces acting on the element. The dynamic differential equations of motion by the standard assembling procedure are obtained. These differential equations are integrated with a selected time step size Δt. The displacements ${}^{n+1}\mathbf{U}$ at end of time step are finally obtained according to equation:

$$\hat{\mathbf{K}}_{\text{tissue}}\,{}^{n+1}\mathbf{U} = {}^{n+1}\hat{\mathbf{F}} \tag{1.8}$$

where the tissue stiffness matrix $\hat{\mathbf{K}}_{\text{tissue}}$ and vector ${}^{n+1}\hat{\mathbf{F}}$ are expressed in terms of the matrices and vector in (1.7). Above equation is obtained under the assumption that the problem is linear: the viscous resistance is constant, displacements are small, and the material is linear elastic.

In many real examples as in case of aneurism or heart ventricle motion, the wall displacements can be large, hence the problem becomes geometrically nonlinear. Also, the tissue of blood vessels has nonlinear constitutive law which has to be expressed with materially nonlinear finite element formulation. Therefore, the linear formulation of the equation may not be appropriate. For a nonlinear problem, there is incremental–iterative equation

$${}^{n+1}\hat{\mathbf{K}}_{\text{tissue}}^{(i-1)}\Delta\mathbf{U}^{(i)} = {}^{n+1}\hat{\mathbf{F}}^{(i-1)} - {}^{n+1}\mathbf{F}^{\text{int}(i-1)} \tag{1.9}$$

Here, $\Delta\mathbf{U}^{(i)}$ are the nodal displacement increments for the iteration "i," and the system matrix ${}^{n+1}\hat{\mathbf{K}}_{\text{tissue}}^{(i-1)}$, the force vector ${}^{n+1}\hat{\mathbf{F}}^{(i-1)}$, and the vector of internal forces ${}^{n+1}\mathbf{F}^{\text{int}(i-1)}$ correspond to the previous iteration.

We described the material nonlinearity of blood vessels which is used in further applications. The geometrically linear part of the stiffness matrix, $\left({}^{n+1}\mathbf{K}_{\text{L}}\right)_{\text{tissue}}^{(i-1)}$, and nodal force vector, ${}^{n+1}\mathbf{F}^{\text{int}(i-1)}$, are defined:

$$\left({}^{n+1}\mathbf{K}_{\text{L}}\right)_{\text{tissue}}^{(i-1)} = \int_{V}\mathbf{B}_{\text{L}}^{T}\,{}^{n+1}\mathbf{C}_{\text{tissue}}^{(i-1)}\mathbf{B}_{\text{L}}\,\mathrm{d}V, \quad \left({}^{n+1}\mathbf{F}^{\text{int}}\right)^{(i-1)} = \int_{V}\mathbf{B}_{\text{L}}^{T}\,{}^{n+1}\boldsymbol{\sigma}^{(i-1)}\mathrm{d}V \tag{1.10}$$

Here, the consistent tangent constitutive matrix ${}^{n+1}\mathbf{C}_{\text{tissue}}^{(i-1)}$ of tissue and the stresses at the end of time step ${}^{n+1}\boldsymbol{\sigma}^{(i-1)}$ depend on the material model used.

1.7.4 FSI Interaction

In many models of cardiovascular examples where deformation of blood vessel walls was taken into account, we can implement the loose coupling approach for the FSI [113–116]. The overall algorithm consists of the following steps:

1) For the current geometry of the blood vessel, determine blood flow (with Arbitrary Lagrangian–Eulerian (ALE) formulation). The boundary conditions for the fluid are wall velocities at the common blood–blood vessel surface.
2) Calculate the loads, which act on the walls from fluid domain (blood).
3) Determine deformation of the walls taking the current loads from the fluid domain (blood).
4) Check for the overall convergence which includes fluid and solid domain. If convergence is reached, go to the next time step. Otherwise go to step (1).
5) Update blood domain geometry and velocities at the common solid–fluid boundary for the new calculation of the fluid domain. In case of large wall displacements, update the finite element mesh for the fluid domain. Go to step (1).

The shear stress and drag force distribution have been presented in Figures 1.2 and 1.3 for two different patients for proximal and distal AAA.

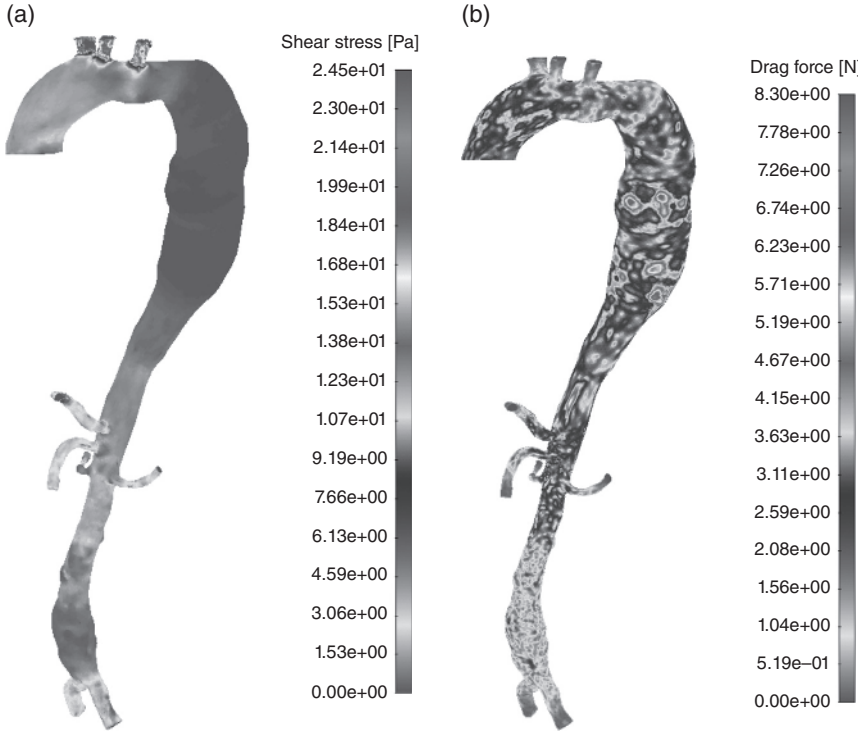

Figure 1.2 (a) Shear stress distribution. (b) Drag force distribution.

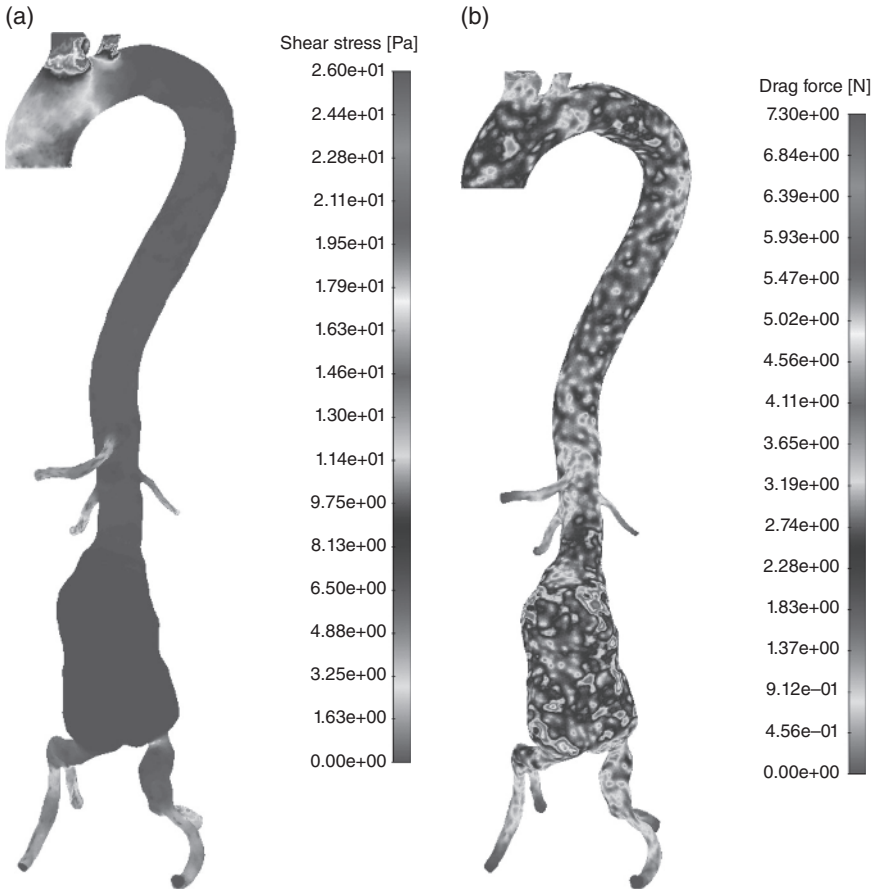

Figure 1.3 (a) Shear stress distribution. (b) Drag force distribution.

1.8 Data Mining and Future Clinical Decision Support System

Together with CFD simulation, there are numerous statistics-based machine learning methods that can be used to give more accurate and faster conclusions for clinicians [117].

Kolachalama et al. [118] proposed a DM technique that accounted for the geometric variability in patients for predicting cardiovascular flows. A Bayesian network-based algorithm was used to understand the influence of key parameters through a sensitivity analysis. Martufi et al. [119] investigated a geometrical characterization of the wall thickness distribution in AAA. They were able to train a

model to differentiate the wall thicknesses in ruptured and un-ruptured AAA. Shum et al. [120] developed a model from 66 ruptured data sets and 10 non-ruptured data sets and their geometric indices and wall thickness variations. The results of this study showed that, in addition to maximum diameter, sac length, sac height, volume, surface area, bulge height, and ILT volume were all highly correlated with rupture status. In this study, the overall classification accuracy was 86.6%. It used a decision tree algorithm that is one of the possible machine learning methods that can be used for large data sets requiring a decision output.

Filipovic et al. [121] combined DM techniques and CFD for the estimation of the wall shear stresses in AAA under prescribed geometry changes. They performed large-scale CFD runs for creating machine learning data on the Grid infrastructure and their results showed that DM models provide good prediction of the shear stress at the AAA in comparison with full CFD model results on real patient data.

The abovementioned studies have been limited by the use of geometric parameters and, in particular, the maximum diameter of lumen alone as factors contributing to the rupture of an AAA. But other parameters such as patient history and comorbidities and presence of stents or other geometric parameters such as the aneurysm neck angles, tortuosity, and genetics factors [122–126] should be included. Despite the fact that state-of-the-art FEM approaches represent powerful tool for estimation of AAA, their application in clinical practice remains limited due to several reasons. Firstly, every patient has specific and complex anatomy and it is not possible to create a general or parametric human model. Moreover, accuracy of simulations depends on the considered level of details, meaning that increasing required computation time and power will be necessary for obtaining precise results. As a consequence, performing patient-specific simulation may take a few hours (if patient scans are available in the first place). This makes current FEM approaches inadequate for urgent situations such as alerting patient in case of AAA rupture.

In order to avoid described limitations, the patient-specific DSS could be proposed. The main idea is to perform patient-specific forward simulations in advance. AAA of different types (sizes and positions) will be simulated and calculated stress analysis will be used for training of intelligent model. But, in order to perform forward FEM simulations patient geometry is required. For this reason, during the registration into our system, in local workstation (user hospital), patient or his/her medical institution will be asked to provide us patients' medical scans (CT or MRI for example), if there are any. However, it is assumed that some patients will not have medical scans.

For future clinical DSS, we suggest the following scenario: new user has already performed medical scanning (CT or MRI) and these data are uploaded to the central server (or they are available over institution existing connection). In that case, we will generate 3D patient-specific FEM model by using image-based modeling software developed on the server. It is important to mention that, for the project

purposes, accurate reconstructions will be necessary only for torso and aorta. We will reconstruct only aorta (by using statistical shape models) and torso interface (by using level set and marching cubes algorithms) because they are needed for setting FEM boundary conditions and because, on the other hand, accurate reconstruction of all organs represents time-consuming and computationally expensive problem with current medical imaging methods. In this way, highly accurate geometry, materials, and boundary conditions could be obtained for every patient (Figure 1.4).

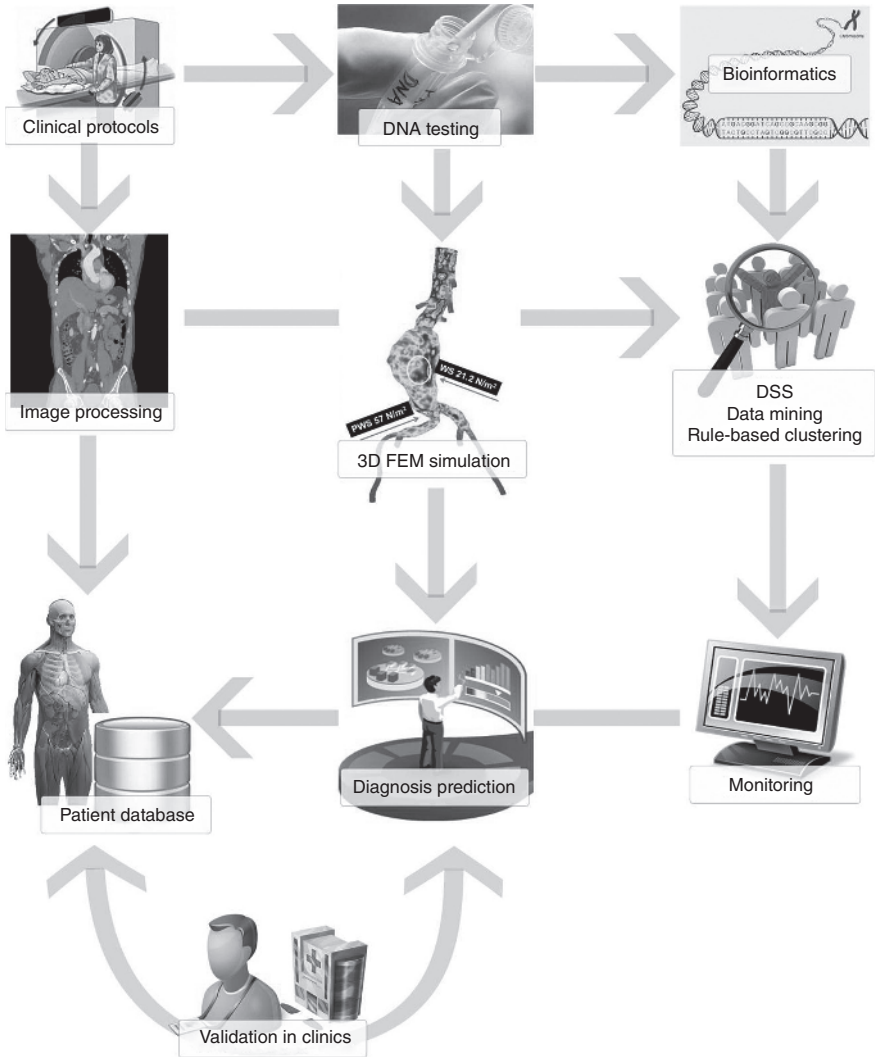

Figure 1.4 Description of clinical decision support system for AAA disease.

1.9 Conclusions

In the first part of this paper, literature survey on AAA biomechanics is reported including several aspects from experimental test, constitutive model, and ILT. Further, we presented our FE models, aimed at simulating and enhancing the computational study of the aneurismatic pathology. The combination of fluid and nonlinear structure modeling can give better understanding of the flow, pressure distribution, wall shear stress quantification, and effect of material properties and geometrical parameters. Computational methods have made patient-specific analyses possible, a feature essential for understanding the progression of AAA in a particular patient. Finally, future clinical DSS is suggested by using DM approach. The main aim is to run predictive FSI model in order to estimate the risk of rupture and to use patient-specific wall properties with calcium, tissue disease, and thrombus to overcome multiple level of uncertainties.

During the last two decades, significant efforts have been made in order to define a computational model which includes biomechanical and biological approach, but still a lot of clinical studies are necessary in order to make these computational studies real in everyday clinical practice.

Exercise 1.1 Modeling of Blood Flow Within the AAA

The shape of AAA is very important. The severity of AAA is commonly estimated in clinical practice by considering the AAA maximal diameter. However, from the mechanical point of view, the hemodynamic effects and the mechanical stresses within the AAA tissue certainly are important in the process of the AAA rupture. Bulge diameter alone may not be a sufficient criterion for determination of rupture risk; therefore, an insight into the hemodynamic effects and the stress–strain quantification and distribution within the vessel wall are of great significance even in medical practice.

Generation of the Finite Element Model

A simplified geometry of an aneurism is shown in Figure 1.5. With the on-web software, the 3D finite element model for the blood flow domain can be parametrically generated. A transition smoothness between the surfaces is achieved by using Bezier's curves. Also, the results can be displayed with a user-friendly menu in a way suitable for an insight into medical aspects of the blood flow conditions. A detailed description of the software use is given on the web (within Tutorial of each example), while the description of geometric parameters is given in the caption of Figure 1.5.

(*Continued*)

Exercise 1.1 (Continued)

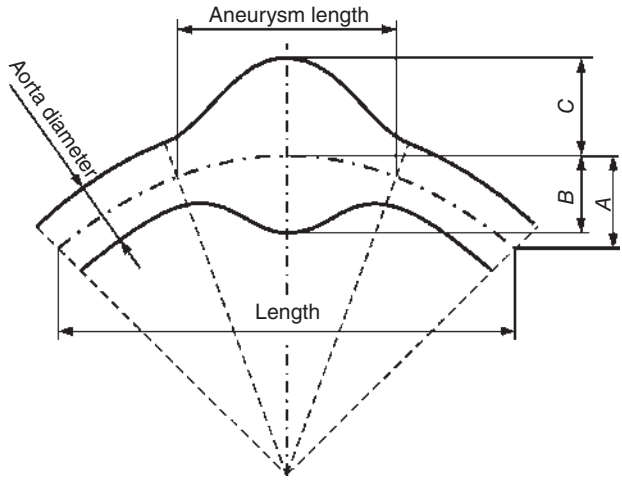

Figure 1.5 Geometrical parameters of AAA: "Length" is the parameter which defines the total horizontal projection of the generated aneurysm model; "*A*" is the height of the arc of central line; "Aorta diameter" is the abdominal aorta diameter; "*B*" is the radius from the central line to the inner wall of the aneurysm; "*C*" is the radius from the central line to the outer wall of the aneurysm; "Aneurysm length" is an average length of the AAA.

Boundary Conditions

At the inflow aorta cross-section, a fully developed parabolic flow is assumed, determined by a selected volume flux. The normal stress and tangential stress are set to be equal to zero (stress-free condition) or they are prescribed at the outlet cross-section.

It is assumed that the entering flow is pulsatile, with a typical waveform shown in Figure 1.6 [127]. As described in the software menu, the waveform can be changed.

Results

Results for two examples of the symmetric AAA are given here: (i) case with rigid walls and (ii) AAA with deformable walls. Results not shown here and solutions for other model parameters can be obtained using Software on the web.

(*Continued*)

Exercise 1.1 (Continued)

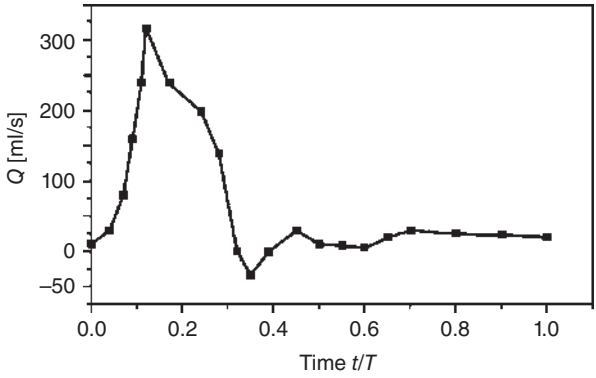

Figure 1.6 A typical in-flow waveform at the aorta entry. Q is the volumetric in-flux and t/T is the relative time with respect to the cycle period T.

Modeling of AAA Assuming Rigid Walls

We analyze an aneurism at the straight aorta domain, where aorta proximal and distal to the AAA bulge is idealized as straight rigid tube and branching arteries are excluded. The model has ratio $D/d = 2.75$ and geometry generated according to Figure 1.5 (D and d are diameters of the bulge and aorta, respectively). The data are: blood density is $\rho = 1.05$ g/cm^3; kinematic viscosity (Newtonian fluid) $\nu = 0.035$ cm^2/s, $d = 12.7$ mm. The inflow velocity is defined by the flux function given in Figure 1.6. The FE mesh consisted of approximately 8000 3D 8-node brick elements.

The results for the velocity and pressure at peak systole $t/T = 0.16$ are shown in Figure 1.7. The velocity disturbance in the region of the aneurism is notable. Also, the region of maximum pressure is located inside AAA.

Modeling AAA with Deformable Walls

Here, an aneurysm of the straight aorta with deformable walls is modeled according to the FSI algorithm. Blood flow is calculated using 2112 eight-node 3D elements, and 264 four-node shell elements used to model the aorta wall, with the wall thickness $\delta = 0.2$ cm. The material constants for blood as in the previous example, while data for the vessel wall are: Young's modulus $E = 2.7$ MPa, Poisson's ratio $\nu = 0.45$, wall thickness $\delta = 0.2$ cm, and tissue density $\rho = 1.1$ g/cm^3. Boundary conditions for the model are prescribed velocity profile (see Figure 1.8a) and output pressure profile as given in Figure 1.8b.

(*Continued*)

Exercise 1.1 (Continued)

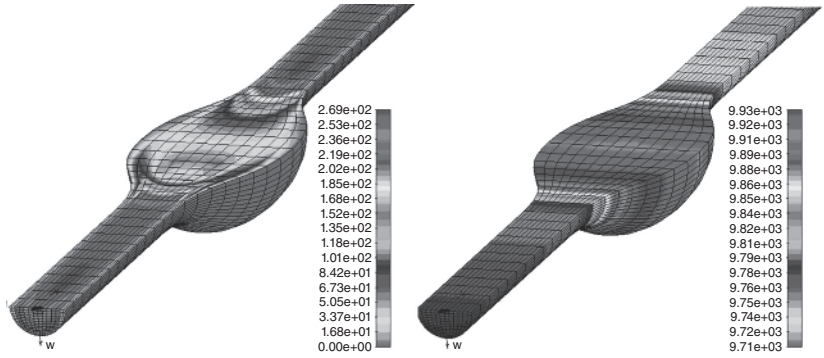

Figure 1.7 Velocity field (left panel) and pressure distribution (right panel) for peak systole $t/T = 0.16$ of AAA for the model with $D/d = 2/75$, $d = 12.7$ mm.

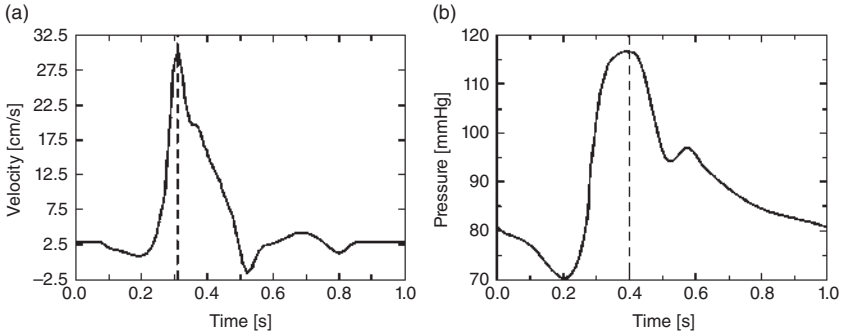

Figure 1.8 Input velocity and output pressure profiles for the AAA on a straight vessel. Inlet peak systolic flow is at $t = 0.305$ s and outlet peak systolic pressure is at $t = 0.4$ s. (a) Velocity waveform; (b) pressure waveform. *Source*: Modified from Scotti et al. [44].

The results for velocity magnitude distribution at $t = 0.305$ s are shown in Figure 1.9a. The von Mises wall stress distributions at $t = 0.4$ s is given in Figure 1.9b. It can be seen that the velocities are low in the domain of the aneurism, while the larger values of the wall stress are at the proximal and distal aneurism zones.

(*Continued*)

Exercise 1.1 (Continued)

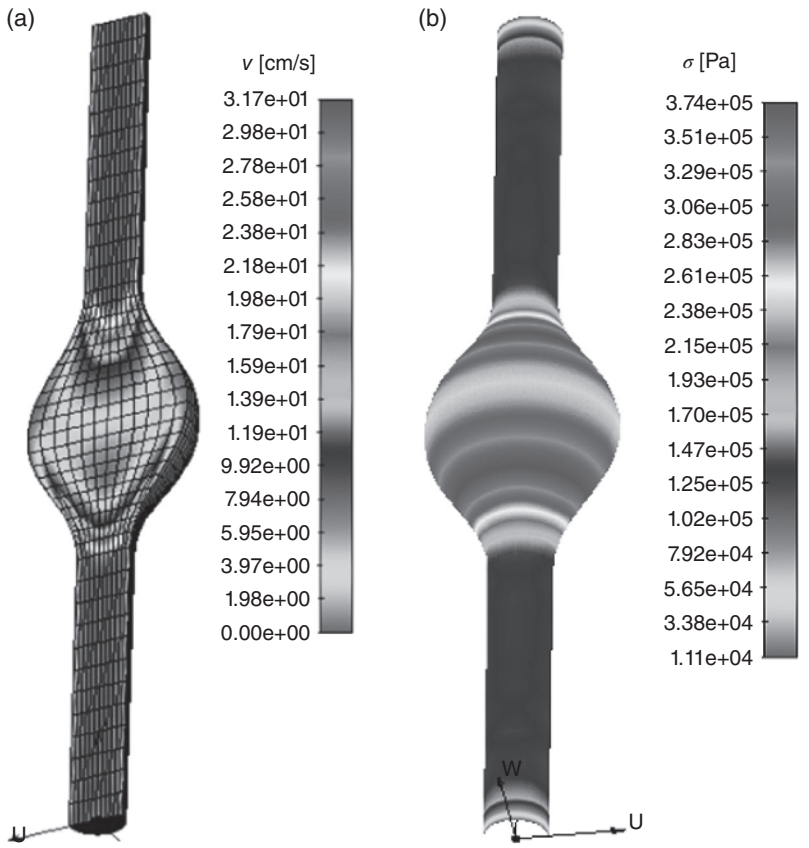

Figure 1.9 Velocity magnitude field and von Mises wall stress distribution for symmetric AAA on the straight vessel. (a) Velocity field distribution for peak at $t = 0.305$ s; (b) von Mises wall stress distributions for blood pressure peak at $t = 0.4$ s.

References

1 McGloughlin, T.M. and Doyle, B.J. (2010). New approaches to abdominal aortic aneurysm rupture risk assessment: engineering insights with clinical gain. *Arterioscler. Thromb. Vasc. Biol.* **30**: 1687–1694. https://doi.org/10.1161/ATVBAHA.110.204529.

2 Fleming, C., Whitlock, E.P., Beil, T., and Lederle, F.A. (2005). Review: screening for abdominal aortic aneurysm: a best-evidence systematic review for the U.S. Preventive Services Task Force. *Ann. Intern. Med.* **142**: 203–211.

3 O'Gara, T.P. (2003). Aortic aneurysm. *Circulation* **107**: e43–e45.

4 Minino, A.M., Heron, M.P., Murphy, S.L., and Kochanek, K.D. (2007). Deaths: final data for 2004. *Nat. Vital. Stat. Rep.* **55**: 1–119.

5 Sakalihasan, N., Limet, R., and Defawe, O.D. (2005). Abdominal aortic aneurysm. *Lancet* **365** (9470): 1577–1589.

6 Thompson, M.M. (2003). Controlling the expansion of abdominal aortic aneurysms. *Br. J. Surg.* **90**: 897–898.

7 Thompson, M.M. (2003). Infrarenal abdominal aortic aneurysms. *Curr. Treat Opt. Cardiovasc. Med.* **5** (2): 137–146.

8 Thompson, R.W. and Baxter, B.T. (1999). MMP inhibition in abdominal aortic aneurysms. Rationale for a prospective randomized clinical trial. *Ann. N. Y. Acad. Sci.* **878**: 159–178.

9 Bown, M.J., Sutton, A.J., Bell, P.R., and Sayers, R.D. (2002). A meta-analysis of 50 years of ruptured abdominal aortic aneurysm repair. *Br. J. Surg.* **89**: 714–730.

10 Venkatasubramaniam, A.K., Fagan, M.J., Mehta, T. et al. (2004). A Comparative Study of Aortic Wall Stress Using Finite Element Analysis for Ruptured and Non-ruptured Abdominal Aortic Aneurysms. *Eur. J. Vasc. Endovasc. Surg.* **28** (2): 168–176.

11 Choke, E., Cockerill, G., Wilson, W.R.W. et al. (2005). A review of biological factors implicated in abdominal aortic aneurysm rupture. *Eur. J. Vasc. Endovasc. Surg.* **30**: 227–244.

12 Fillinger, M.F., Marra, S.P., Raghavan, M.L., and Kennedy, F.E. (2003). Prediction of rupture risk in abdominal aortic aneurysm during observation: wall stress versus diameter. *J. Vasc. Surg.* **37**: 724–732.

13 Fillinger, M.F., Raghavan, M.L., Marra, S.P. et al. (2002). In vivo analysis of mechanical wall stress and abdominal aortic aneurysm rupture risk. *J. Vasc. Surg.* **36**: 589–597.

14 Upchurch, G.R. Jr. and Schaub, T.A. (2006). Abdominal aortic aneurysm. *Am. Fam. Phys.* **73**: 1198–1204.

15 Sonesson, B., Sandgren, T., and Lanne, T. (1999). Abdominal aortic aneurysm wall mechanics and their relation to risk of rupture. *Eur. J. Vasc. Endovasc. Surg.* **18**: 487–493.

16 Doyle, B.J., Callanan, A., Walsh, M.T. et al. (2009). A finite element analysis rupture index (FEARI) as an additional tool for abdominal aortic aneurysm rupture prediction. *Vasc. Dis. Prev.* **6**: 114–121.

17 Doyle, B.J., Cloonan, A.J., Walsh, M.T. et al. (2010). Identification of rupture locations in patient-specific abdominal aortic aneurysms using experimental and computational techniques. *J. Biomech.* **43**: 1408–1416.

18 Doyle, B.J., Corbett, T.J., Callanan, A. et al. (2009). An experimental and numerical comparison of the rupture locations of an abdominal aortic aneurysm. *J. Endovasc. Ther.* **16**: 322–335.

19 Doyle, B.J., Grace, P.A., Kavanagh, E.G. et al. (2009). Improved assessment and treatment of abdominal aortic aneurysms: the use of 3D reconstructions as a surgical guidance tool in endovascular repair. *Ir. J. Med. Sci.* **178**: 321–328.

20 Biasetti, J. and Gasser, T.C. (2012). A fluido-chemical model to predict the growth of intra-luminal thrombus in abdominal aortic aneurysms, ECCOMAS 2012. *6th European Congress on Computational Methods in Applied Sciences and Engineering*, Vienna, Austria (10–14 September 2012).

21 Biasetti, J., Gasser, T.C., Auer, M. et al. (2010). Hemodynamics of the normal aorta compared to fusiform and saccular abdominal aortic aneurysms with emphasis on a potential thrombus formation mechanism. *Ann. Biomed. Eng.* **38** (2): 380–390.

22 Georgakarakos, E., Ioannou, C., Kamarianakis, Y. et al. (2010). The role of geometric parameters in the prediction of abdominal aortic aneurysm wall stress. *Eur. J. Vasc. Endovasc. Surg.* **39**: 42–48.

23 Georgakarakos, E., Ioannou, C.V., Papaharilaou, Y. et al. (2013). Peak wall stress does not necessarily predict the location of rupture in abdominal aortic aneurysms. *Eur. J. Vasc. Endovasc. Surg.* **39** (3): 302–304.

24 Vorp, D.A. (2007). Biomechanics of abdominal aortic aneurysm. *J. Biomech.* **40**: 1887–1902.

25 VASCOPS Vascular Diagnostics (2007). On-line survey: clinical assessment of AAA rupture risk: are biomechanical predictors needed? http://www.vascops.com (accessed 12 September 2021).

26 Alcorn, H.G., Wolfson, S.K. Jr., Sutton-Tyrrell, K. et al. (1996). Risk factors for abdominal aortic aneurysms in older adults enrolled in The Cardiovascular Health Study. *Arterioscler. Thromb. Vasc. Biol.* **16**: 963–970.

27 Derubertis, B.G., Trocciola, S.M., Ryer, E.J. et al. (2007). Abdominal aortic aneurysm in women: prevalence, risk factors, and implications for screening. *J. Vasc. Surg.* **46**: 630–635.

28 Forsdahl, S.H., Singh, K., Solberg, S. et al. (2009). Risk factors for abdominal aortic aneurysms: a 7-year prospective study: the Tromso Study, 1994–2001. *Circulation* **119**: 2202–2208.

29 Svensjo, S., Bjorck, M., and Wanhainen, A. (2013). Current prevalence of abdominal aortic aneurysm in 70-year-old women. *Br. J. Surg.* **100**: 367–372.

30 Lederle, F.A., Johnson, G.R., Wilson, S.E. et al. (2001). Abdominal aortic aneurysm in women. *J. Vasc. Surg.* **34**: 122–126.

31 Singh, K., Bonaa, K.H., Jacobsen, B.K. et al. (2001). Prevalence of and risk factors for abdominal aortic aneurysms in a population-based study: the Tromso Study. *Am. J. Epidemiol.* **154**: 236–244.

32 Kent, K.C., Zwolak, R.M., Egorova, N.N. et al. (2010). Analysis of risk factors for abdominal aortic aneurysm in a cohort of more than 3 million individuals. *J. Vasc. Surg.* **52**: 539–548.

33 Lederle, F.A., Johnson, G.R., Wilson, S.E. et al. (2000). The aneurysm detection and management study screening program: validation cohort and final results. Aneurysm Detection and Management Veterans Affairs Cooperative Study Investigators. *Arch. Intern. Med.* **160**: 1425–1430.

34 Lederle, F.A., Nelson, D.B., and Joseph, A.M. (2003). Smokers' relative risk for aortic aneurysm compared with other smoking-related diseases: a systematic review. *J. Vasc. Surg.* **38**: 329–334.

35 Jahangir, E., Lipworth, L., Edwards, T.L. et al. (2015). Smoking, sex, risk factors and abdominal aortic aneurysms: a prospective study of 18 782 persons aged above 65 years in the Southern Community Cohort Study. *J. Epidemiol. Community Health* **69** (5): 481–488.

36 Darling, R.C., Messina, C.R., Brewster, D.C., and Ottinger, L.W. (1977). Autopsy study of unoperated abdominal aortic aneurysms. The case for early resection. *Circulation* **56** (Suppl. 3): 161–164.

37 Stringfellow, M.M., Lawrence, P.F., and Stringfellow, R.G. (1987). The influence of aorta-aneurysm geometry upon stress in the aneurysm wall. *J. Surg. Res.* **42**: 425–433.

38 Vorp, D.A., Raghavan, M.L., and Webster, M. (1998). Mechanical wall stress in abdominal aortic aneurysm: inuence of diameter and asymmetry. *J. Vasc. Surg.* **27**: 632–639.

39 Raghavan, M.L. and Vorp, D.A. (2000). Toward a biomechanical tool to evaluate rupture potential of abdominal aortic aneurysm: identification of a finite strain constitutive model and evaluation of its applicability. *J. Biomech.* **33** (4): 475–482.

40 Raghavan, M.L., Kratzberg, J., Castro de Tolosa, E.M. et al. (2006). Regional distribution of wall thickness and failure properties of human abdominal aortic aneurysm. *J. Biomech.* **39**: 3010–3016.

41 Raghavan, M.L., Vorp, D.A., Federle, M.P. et al. (2000). Wall stress distribution on three-dimensionally reconstructed models of human abdominal aortic aneurysm. *J. Vasc. Surg.* **31**: 760–769.

42 Vande Geest, J.P., Sacks, M.S., and Vorp, D.A. (2006). A planar biaxial constitutive relation for the luminal layer of intra-luminal thrombus in abdominal aortic aneurysms. *J. Biomech.* **39**: 2347–2354.

43 Scotti, C.M., Jimenez, J., Muluk, S.C., and Finol, E.A. (2008). Wall stress and flow dynamics in abdominal aortic aneurysms: finite element analysis vs. fluid–structure interaction. *Comput. Methods Biomech. Biomed. Eng.* **11** (3): 301–322.

44 Scotti, C.M., Shkolnik, A.D., Muluk, S., and Finol, E.A. (2005). Fluid–structure interaction in abdominal aortic aneurysms: effects of asymmetry and wall thickness. *Biomed. Eng. Online* **4** (4): 64.

45 Finol, E.A. and Amon, C.H. (2001). Blood flow in abdominal aortic aneurysms: pulsatile flow hemodynamics. *J. Biomech. Eng.* **123**: 474–484.

46 Finol, E.A. and Amon, C.H. (2002). Flow-induced wall shear stress in abdominal aortic aneurysms: part I – steady flow hemodynamics. *Comput. Methods Biomech. Biomed. Eng.* **5** (4): 309–318.

47 Federico, S. and Gasser, T.C. (2010). Nonlinear elasticity of biological tissues with statistical fiber orientation. *J. R. Soc. Interf.* **7** (47): 955–966.

48 Hardin, R.H. and Sloane, N.J.A. (1996). McLaren's improved snub cube and other new spherical designs in three dimentions. *Discret. Comput. Geom.* **15**: 429–441.

49 Zhang, Y., Barocas, V.H., Berceli, S.A. et al. (2016). Multi-scale modeling of the cardiovascular system: disease development, progression, and clinical intervention. *Ann. Biomed. Eng.* **44** (9): 2642–2660.

50 Guidoboni, G., Glowinski, R., Cavallini, N. et al. (2009). A kinematically coupled time-splitting scheme for fluid–structure interaction in blood flow. *Appl. Math. Lett.* **22** (5): 684–688.

51 Guidoboni, G., Glowinski, R., Cavallini, N., and Čanić, S. (2009). Stable loosely-coupled-type algorithm for fluid–structure interaction in blood flow. *J. Comput. Phys.* **228** (18): 6916–6937.

52 Bukač, M., Čanić, S., Glowinski, R. et al. (2013). Fluid–structure interaction in blood flow capturing non-zero longitudinal structure displacement. *J. Comput. Phys.* **235**: 515–541.

53 Quarteroni, A. and Formaggia, L. (2004). Mathematical modelling and numerical simulation of the cardiovascular system in modelling of living systems. In: *12 of Handbook of Numerical Analysis*, 3–127. Amsterdam: North-Holland.

54 Formaggia, L., Gerbeau, J.F., Nobile, F., and Quarteroni, A. (2001). On the coupling of 3D and 1D Navier–Stokes equations for flow problems in compliant vessels. *Comput. Methods Appl. Mech. Eng.* **191** (6–7): 561–582.

55 Formaggia, L., Lamponi, D., and Quarteroni, A. One-dimensional models for blood flow in arteries. *J. Eng. Math.* **47** (3–4): 251–276.

56 Nobile, F. and Vergara, C. (2008). An effective fluid–structure interaction formulation for vascular dynamics by generalized Robin conditions. *SIAM J. Sci. Comput.* **30** (2): 731–763.

57 Causin, P., Gerbeau, J.F., and Nobile, F. (2005). Added-mass effect in the design of partitioned algorithms for fluid–structure problems. *Comput. Methods Appl. Mech. Eng.* **194** (42–44): 4506–4527.

58 Čanić, S., Mikelić, A., and Tambača, J. (2005). A two-dimensional effective model describing fluid–structure interaction in blood flow: analysis, simulation and experimental validation. *Comptes Rendus.* **333** (12): 867–883.

59 Čanić, S., Tambača, J., Guidoboni, G. et al. (2006). Modeling viscoelastic behavior of arterial walls and their interaction with pulsatile blood flow. *SIAM J. Appl. Math.* **67** (1): 164–193.

60 Čanić, S., Hartley, C.J., Rosenstrauch, D. et al. (2006). Blood flow in compliant arteries: an effective viscoelastic reduced model, numerics, and experimental validation. *Ann. Biomed. Eng.* **34** (4): 575–575.

61 Heil, A., Hazel, L., and Boyle, J. (2008). Solvers for large-displacement fluid–structure interaction problems: segregated versus monolithic approaches. *Comput. Mech.* **43** (1): 91–101.

62 MacSweeney, S.T.R., Powell, J.T., and Greenhalgh, R.M. (1994). Pathogenesis of abdominal aortic aneurysm. *Br. J. Surg.* **81**: 935–941.

63 van't Veer, M., Buth, J., Merkx, M. et al. (2008). Biomechanical properties of abdominal aortic aneurysms assessed by simultaneously measured pressure and volume changes in humans. *J. Vasc. Surg.* **48** (6): 1401–1407.

64 Ganten, M.K., Krautter, U., von Tengg-Kobligk, H. et al. (2008). Quantification of aortic distensibility in abdominal aortic aneurysm using ecg-gated multi-detector computed tomography. *Vasc. Intervent.* **18** (5): 966–973.

65 Molacek, J., Baxa, J., Houdek, K. et al. (2011). Assessment of abdominal aortic aneurysm wall distensibility with electrocardiography-gated computed tomography. *Ann. Vasc. Surg.* **25** (8): 1036–1042.

66 Di Puccio, F., Celi, S., and Forte, P. (2012). Review of experimental investigations on compressibility of arteries and the introduction of a new apparatus. *Exp. Mech.* **52** (7): 1–8. https://doi.org/10.1007/s11340-012-9614-4.

67 Humphrey, J.D. and Yin, F.C. (1987). A new constitutive formulation for characterizing the mechanical behavior of soft tissues. *Biophys. J.* **52** (4): 563–570.

68 Ogden, R.W. (2009). Anisotropy and nonlinear elasticity in arterial wall mechanics. In: *Biomechanical Modelling at the Molecular, Cellular and Tissue Levels. CISM Courses and Lectures*, vol. **508** (eds. G.A. Holzapfel, R.W. Ogden, F. Pfeiffer, et al.), 179–258. Vienna: Springer.

69 Vande Geest, J.P., Sacks, M.S., and Vorp, D.A. (2004). Age dependency of the biaxial biomechanical behavior of human abdominal aorta. *J. Biomech. Eng.* **12**: 815–822.

70 Vande Geest, J.P., Sacks, M.S., and Vorp, D.A. (2006). The effects of aneurysm on the biaxial mechanical behavior of human abdominal aorta. *J. Biomech.* **39**: 1324–1334.

71 Koncar, I., Nikolic, D., Pantovic, S. et al. (2013). Modeling of abdominal aortic aneurysm rupture by using bubble inflation test. *Bioinform. Bioeng. (BIBE)* https://doi.org/10.1109/BIBE.2013.6701612.

72 Vande Geest, J.P., Di Martino, E.S., Bohra, A. et al. (2006). A biomechanics-based rupture potential index for abdominal aortic aneurysm risk assessment. *Ann. N. Y. Acad. Sci.* **1085**: 11–21.

73 Thubrikar, M.J., Labrosse, M., Robicsek, F. et al. (2001). Mechanical properties of abdominal aortic aneurysm wall. *J. Med. Eng. Techn.* **25** (4): 133–142.

74 Stamatopoulos, C., Mathioulakis, D.S., Papaharilaou, Y., and Katsamouris, A. (2011). Experimental unsteady flow study in a patientspecific abdominal aortic aneurysm model. *Exp. Fluids* **50** (6): 1695–1709.

75 Holzapfel, G.A. (2006). Determination of material models for arterial walls from uniaxial extension tests and histological structure. *J. Theor. Biol.* **238** (2): 290–302.

76 Simsek, F.G. and Kwon, Y.W. (2015). Investigation of material modeling in fluid–structure interaction analysis of an idealized three layered abdominal aorta: aneurysm initiation and fully developed aneurysms. *J. Biol. Phys.* **41** (2): 173–201.

77 Taghizadeh, H., Tafazzoli-Shadpour, M., Shadmehr, M., and Fatouraee, N. (2015). Evaluation of biaxial mechanical properties of aortic media based on the lamellar microstructure. *Materials* **8** (1): 302–316.

78 Sokolis, D.P., Kefaloyannis, E.M., Kouloukoussa, M. et al. (2006). A structural basis for the aortic stress–strain relation in uniaxial tension. *J. Biomech.* **39** (9): 1651–1662.

79 Karimi, A., Navidbakhsh, M., Shojaei, A., and Faghihi, S. (2013). Measurement of the uniaxial mechanical properties of healthy and atherosclerotic human coronary arteries. *Mater. Sci. Eng. C* **33** (5): 2550–2554.

80 Taylor, C.A. and Humphrey, J.D. (2009). Open problems in computational vascular biomechanics: hemodynamics and arterial wall mechanics. *Comput. Methods Appl. Mech. Eng.* **198** (45–46): 3514–3523.

81 Raut, S.S., Chandra, S., Shum, J., and Finol, E.A. (2013). The role of geometric and biomechanical factors in abdominal aortic aneurysm rupture risk assessment. *Ann. Biomed. Eng.* **41** (7): 1459–1477.

82 Stenbaek, J., Kalin, B., and Swedenborg, J. (2000). Growth of thrombus may be a better predictor of rupture than diameter in patients with abdominal aortic aneurysms. *Eur. J. Vasc. Endovasc. Surg.* **20** (5): 466–469.

83 Li, Z.-Y., U-King-Im, J., Tang, T.Y. et al. (2008). Impact of calcification and intraluminal thrombus on the computed wall stresses of abdominal aortic aneurysm. *J. Vasc. Surg.* **47** (5): 928–936.

84 Di Martino, E.S. and Vorp, D.A. (2003). Effect of variation in intraluminal thrombus constitutive properties on abdominal aortic aneurysm wall stress. *Ann. Biomed. Eng.* **31** (7): 804–809.

85 O'Leary, S.A., Kavanagh, E.G., Grace, P.A. et al. (2014). The biaxial mechanical behaviour of abdominal aortic aneurysm intraluminal thrombus: classification of morphology and the determination of layer and region specific properties. *J. Biomech.* **47** (6): 1430–1437.

86 Tong, J., Schriefl, A.J., Cohnert, T., and Holzapfel, G.A. (2013). Gender differences in biomechanical properties, thrombus age, mass fraction and clinical factors of abdominal aortic aneurysms. *Eur. J. Vasc. Endovasc. Surg.* **45** (4): 364–372.

87 Speelman, L., Bosboom, E.M.H., Schurink, G.W.H. et al. (2008). Patient-specific AAA wall stress analysis: 99-percentile versus peak stress. *Eur. J. Vasc. Endovasc. Surg.* **36**: 668–676.

88 Speelman, L., Bosboom, E.M.H., Schurink, G.W.H., Jacobs, M.J.H.M., and van de Vosse, F.N. (2008). *AAA Growth Predicted with Wall Stress. Poster Session Presented at Conference*. Mate Poster Award 2008: 13th Annual Poster Contest.

89 Speelman, L., Hellenthal, F.A., Pulinx, B. et al. (2010). The influence of wall stress on AAA growth and biomarkers. *Eur. J. Vasc. Surg.* **39**: 410–416.

90 Kontopodis, N., Metaxa, E., Papaharilaou, Y. et al. (2013). Changes in geometric configuration and biomechanical parameters of a rapidly growing abdominal aortic aneurysm may provide insight in aneurysms natural history and rupture risk. *Theor. Biol. Med. Model.* **10**: 67.

91 Yushkevich, P.A., Piven, J., Hazlett, H.C. et al. (2006). User-guided 3D active contour segmentation of anatomical structures: significantly improved efficiency and reliability. *NeuroImage* **31**: 1116–1128.

92 Anton, R., Chen, C.Y., Hung, M.Y. et al. (2015). Experimental and computational investigation of the patient-specific abdominal aortic aneurysm pressure field. *Comput. Methods Biomech. Biomed. Eng.* **18** (9): 981–992. https://doi.org/10.1080/10255842.2013.865024.

93 Frauenfelder, T., Lotfey, M., Boehm, T., and Wildermuth, S. (2006). Computational fluid dynamics: hemodynamic changes in abdominal aortic aneurysm after stent-graft implantation. *Cardiovasc. Intervent. Radiol.* **29**: 613–623.

94 Peattie, R.A., Riehle, T.J., and Bluth, E.I. (2004). Pulsatile flow in fusiform models of abdominal aortic aneurysms: flow fields, velocity patterns and flow-induced wall stresses. *J. Biomech. Eng.* **126**: 438–446.

95 Dorfmann, A., Wilson, C., Edgar, E.S., and Peattie, R.A. (2010). Evaluating patient-specific abdominal aortic aneurysm wall stress based on flow-induced loading. *Biomech. Model. Mechanobiol.* **9**: 127–139.

96 Polzer, S., Gasser, T.C., Markert, B. et al. (2012). Impact of poroelasticity of intraluminal thrombus on wall stress of abdominal aortic aneurysms. *Biomed. Eng. Online* **11**: 62.

97 Gasser, T.C., Gorgulu, G., Folkesson, M., and Swedenborg, J. (2008). Failure properties of intraluminal thrombus in abdominal aortic aneurysm under static and pulsating mechanical loads. *J. Vasc. Surg.* **48**: 179–188.

98 Gasser, T.C., Auer, M., Labruto, F. et al. (2010). Biomechanical rupture risk assessment of abdominal aortic aneurysms: model complexity versus predictability of finite element simulations. *Eur. J. Vasc. Endovasc. Surg.* **40**: 176–185.

99 Wang, D.H.J., Makaroun, M.S., Webster, M.W., and Vorp, D.A. (2002). Effect of intraluminal thrombus on wall stress in patient specific models of abdominal aortic aneurysm. *J. Vasc. Surg.* **I36**: 598–604.

100 Wang, D.H., Makaroun, M.S., Webster, M.W., and Vorp, D.A. (2001). Mechanical properties and microstructure of intraluminal thrombus from abdominal aortic aneurysm. *J. Biomech. Eng.* **123**: 536–539.

101 Ayyalasomayajula, A., Vande Geest, J.P., and Simon, B.R. (2010). Porohyperelastic finite element modeling of abdominal aortic aneurysms. *J. Biomech. Eng.* **132**: 104502.

102 Baek, S., Zambrano, B.A., Choi, J., and Lim, C.-Y. (2014). Growth prediction of abdominal aortic aneurysms and its association of intraluminal thrombus. *11th World Congress on Computational Mechanics (WCCM XI); 5th European Conference on Computational Mechanics (ECCM V); 6th European Conference on Computational Fluid Dynamics (ECFD VI)*, Barcelona, Spain (20–25 July 2014).

103 Zeinali-Davarani, S. and Baek, S. (2012). Medical image-based simulation of abdominal aortic aneurysm growth. *Mech. Res. Commun.* **42**: 107–117.

104 Vorp, D.A., Lee, P.C., Wang, D.H. et al. (2001). Association of intraluminal thrombus in abdominal aortic aneurysm with local hypoxia and wall weakening. *J. Vasc. Surg.* **34**: 291–299.

105 Biasetti, J. (2013). Physics of blood flow in arteries and its relation to intra-luminal thrombus and atherosclerosis. Doctoral dissertation no. 84. KTH School of Engineering Sciences, Department of Solid Mechanics – vascuMECH, KTH Royal Institute of Technology, SE-100 44 Stockholm, Sweden.

106 Jones, K.C. and Mann, K.G. (1994). A model for the tissue factor pathway to thrombin.II. A mathematical simulation. *J. Biol. Chem.* **269**: 23367–23373.

107 Filipovic, N., Milasinovic, D., Zdravkovic, N. et al. (2011). Impact of aortic repair based on flow field computer simulation within the thoracic aorta. *Comput. Methods Prog. Biomed.* **101** (3): 243–252.

108 Filipovic, N., Mijailovic, S., Tsuda, A., and Kojic, M. (2006). An implicit algorithm within the arbitrary Lagrangian–Eulerian formulation for solving incompressible fluid flow with large boundary motions. *Comp. Meth. Appl. Mech. Engrg.* **195**: 6347–6361.

109 Filipovic, N., Kojic, M., Ivanovic, M. et al. (2006). *MedCFD, Specialized CFD Software for Simulation of Blood Flow Through Arteries*. Serbia: University of Kragujevac.

110 Perktold, K. and Rappitsch, G. (1995). Computer simulation of local blood flow and vessel mechanics in a compliant carotid artery bifurcation model. *J. Biomech.* **28**: 845–856.

111 Figueroa, C.A., Taylor, C.A., Yeh, V. et al. (2009). Effect of curvature on displacement forces acting on aortic endografts: a 3-dimensional computational analysis. *J. Endovasc. Ther.* **16**: 284–294.

112 Figueroa, C.A., Taylor, C.A., Chiou, A.J. et al. (2009). Magnitude and direction of pulsatile displacement forces acting on thoracic aortic endografts. *J. Endovasc. Ther.* **16**: 350–358.

113 Filipovic, N., Rosic, M., Tanaskovic, I. et al. (2012). ARTreat project: Three-dimensional numerical simulation of plaque formation and development in the arteries. *IEEE Trans. Inf. Technol. Biomed.* **16** (2): 272–278.

114 Filipovic, N. and Schima, H. (2011). Numerical simulation of the flow field within the aortic arch during cardiac assist. *Artif. Organs* **35** (4): 73–83.

115 Veljkovic, D., Filipovic, N., and Kojic, M. (2012). The effect of asymmetry and axial prestraining on the amplitude of mechanical stresses in abdominal aortic aneurysm. *J. Mech. Med. Biol.* **12** (5): 1250089.

116 Krsmanovic, D., Koncar, I., Petrovic, D. et al. (2012). Computer modelling of maximal displacement forces in endoluminal thoracic aortic stent graft. *Comput. Methods Biomech. Biomed. Eng.* **17** (9): 1012–1020.

117 Hastie, T., Tibshirani, R., and Friedman, J. (2008). *The Elements of Statistical Learning: Data Mining, Inference, and Prediction*, Springer Series in Statistics, 2e. New York, NY, USA: Springer.

118 Kolachalama, V.B., Bressloff, N.W., and Nair, P.B. (2007). Mining data from hemodynamic simulations via Bayesian emulation. *Biomed. Eng. Online* **6**: 47.

119 Martufi, G., DiMartino, E.S., Amon, C.H. et al. (2009). Three-dimensional geometrical characterization of abdominal aortic aneurysms: image-based wall thickness distribution. *J. Biomech. Eng.* **131** (6): 061015.

120 Shum, J., Martufi, G., di Martino, E. et al. (2011). Quantitative assessment of abdominal aortic aneurysm geometry. *Ann. Biomed. Eng.* **39** (1): 277–286.

121 Filipovic, N., Ivanovic, M., Krstajic, D., and Kojic, M. (2011). Hemodynamic flow modeling through an abdominal aorta aneurysm using data mining tools. *IEEE Trans. Inf. Technol. Biomed.* **15** (2): 189–194.

122 Pannu, H., Fadulu, V.T., Chang, J. et al. (2005). Mutations in transforming growth factor-beta receptor type II cause familial thoracic aortic aneurysms and dissections. *Circulation* **112**: 513–520.

123 Zhu, L., Vranckx, R., Van Kien, P.K. et al. (2006). Mutations in myosin heavy chain 11 cause a syndrome associating thoracic aortic aneurysm/aortic dissection and patent ductus arteriosus. *Nat. Genet.* **38**: 343–349.

124 Renard, M., Callewaert, B., Baetens, M. et al. (2013). Novel MYH11 and ACTA2 mutations reveal a role for enhanced TGFß signaling in FTAAD. *Int. J. Cardiol.* **165** (2): 314–321.

125 Guo, D.C., Pannu, H., Tran-Fadulu, V. et al. (2007). Mutations in smooth muscle alpha-actin (ACTA2) lead to thoracic aortic aneurysms and dissections. *Nat. Genet.* **39**: 1488–1493.

126 van de Laar, I.M.B.H., Oldenburg, R.A., Pals, G. et al. (2011). Mutations in SMAD3 cause a syndrome form of aortic aneurysms and dissections with early-onset osteoarthritis. *Nat. Genet.* **43**: 121–126.

127 Ku, D.N. (1997). Blood flow in arteries. *Annu. Rev. Fluid Mech.* **29**: 399–434.